Journal of Geochemical Exploration 184 (2018) 247–254

Contents lists available at ScienceDirect

Journal of Geochemical Exploration

journal homepage: www.elsevier.com/locate/gexplo

Removal of As(V) and Sb(V) in water using magnetic nanoparticle-supported layered double hydroxide nanocomposites

Sang-Ho Lee, Heechul Choi, Kyoung-Woong Kim *

School of Environmental Science and Engineering, Gwangju Institute of Science and Technology, Gwangju, Republic of Korea

ARTICLE INFO

Article history:
Received 30 April 2016
Revised 7 September 2016
Accepted 19 November 2016
Available online 21 November 2016

Keywords:
Layered double hydroxide
Magnetic nanoparticle (γ-Fe_2O_3)
Antimony
Arsenic
Reconstruction
Regeneration

ABSTRACT

To remove As(V) and Sb(V) in water, magnetic nanoparticles (MNPs) supported calcined layered double oxide (MLDO) was prepared in order to enhance the separability and removal capacity. MLDO was successfully prepared using a flocculation method and the MNPs stably attached onto the surface of LDH by both chemical bonding and physical attachment. MLDO rapidly separated As(V) and Sb(V) from water due to its external magnetic field, with the saturation magnetism of raw MNPs and MLDO being 63.2 emu/g and 14.3 emu/g, respectively. In addition, MLDO enhanced the removal capacity for As(V) and Sb(V) by reconstruction process. A kinetic study revealed that the removal of As(V) and Sb(V) rapidly reached equilibrium within 120 min for an initial concentration of 50 mg/L, and that the maximum removal capacities for As(V) and Sb(V) as calculated from the Langmuir isotherm are 83.01 mg/g and 180.96 mg/g, respectively. The regeneration rate of As(V) could be maintained at about 70% for five regeneration cycles for 0.5 M NaOH and 5 M NaCl solutions, whereas Sb(V) displayed a lower regenerability due to its higher irreversible fraction in MLDO. Nevertheless, the effective removal efficiency for As(V) and Sb(V), with its easy magnetic separation, implies that MLDO has a potential for use in field applications of wastewater treatment.

1. Introduction

Arsenic (As) and antimony (Sb) are representative toxic metalloids, and occur in groundwater throughout natural and anthropogenic sources (Filella et al., 2002; Smedley and Kinniburgh, 2002). In recent years, there has been a considerable contamination of As(V) and Sb(V) in the groundwater found in several countries around the world. Since severe As(V) contamination in drinking water reported in India and Bangladesh (Chowdhury et al., 2000), broad contamination of As(V) in drinking water in South-East Asian countries such as Vietnam (Hanh et al., 2011), Cambodia (Phan et al., 2013), and Laos (Chanpiwat et al., 2011) have been observed, resulting in acute and chronic toxicity being reported in residents who drink the As(V)-contaminated water. The As(V) contamination in South-East Asian countries is mainly caused by geological properties in which As(V) continuously leaches out from As(V)-containing minerals in groundwater (McCarty et al., 2011). Previous studies (Chanpiwat et al., 2011; Phan et al., 2013; Smith et al., 2000) have already reported that 100–2000 μg/L of As(V) in groundwater has been observed in Bangladesh, Cambodia, and Vietnam. In terms of Sb(V), the contamination has been caused by the insufficient disposal of Sb-bearing wastes, especially in areas of mining and smelting (Jana et al., 2012). Although the toxicity of Sb(V) is less than that of As(V) which has fatal toxicity, the acute and chronic toxicity of Sb(V) occurs respiratory irritation, pneumoconiosis and gastrointestinal symptoms (Sundar and Chakravarty, 2010). In particular, Sb(V) contamination has been observed in Hunan province, China, where 5000 mg/kg of Sb(V) was reported in the soil and 100 μg/L to 7000 μg/L was reported in the surface water and groundwater (He, 2007). Due to the increasing awareness of hazardous effect of As(V) and Sb(V) on humans, these compounds are considered as strong carcinogens and priority pollutants. To this end, the United States Environmental Protection Agency (USEPA) has suggested that the maximum standard of As(V) should be regulated to 10 μg/L (USEPA, 2001) and the World Health Organization guidelines for drinking water standards has assigned a maximum allowable Sb(V) concentration of 5 μg/L (WHO, 2003).

To remove anionic contaminants from drinking water, adsorption and ion exchange processes have been widely applied due to their cost-effectiveness and installation convenience (Mohan and Pittman, 2007). Recently, nanomaterials such as iron oxide (Ray and Shipley, 2015), zero-valent iron (Du et al., 2013), and titanium dioxide (Xu et al., 2005) have been widely applied to the remediation of drinking water because of their high reactivity and selectivity to anionic contaminants. However, the largest problem of concerning the use of nanomaterials in wastewater treatment is that nanoparticles cannot be easily separated after the removal of contaminants; hence, nanomaterials have been applied through alternative methods such as

* Corresponding author.
E-mail address: kwkim@gist.ac.kr (K.-W. Kim).

http://dx.doi.org/10.1016/j.gexplo.2016.11.015
0375-6742/

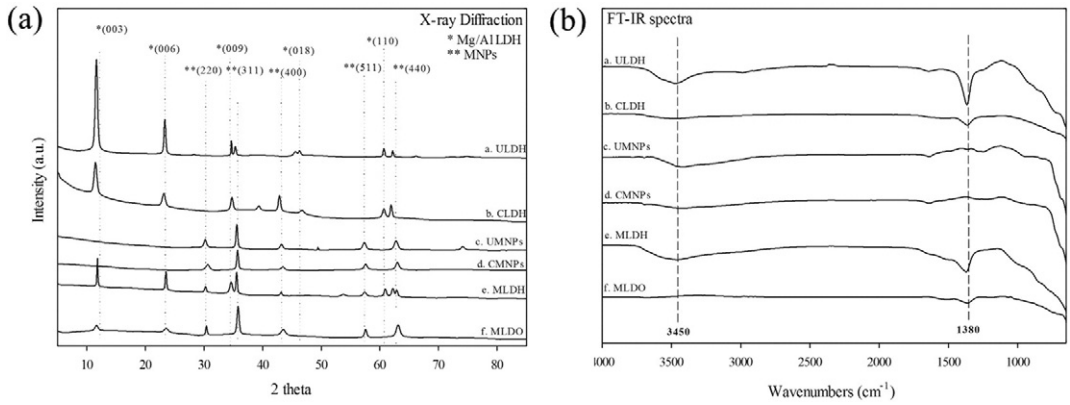

Fig. 1. X-ray diffraction patterns (a) and Fourier transform infrared spectroscopy (b) of ULDH, CLDH, UMNPs, CMNPs, MLDH, and MLDO.

granulation and coatings on fabric—which have a lower removal capacity. Due to problems associated with the use of nanomaterials in the remediation of contaminated water, magnetic nanomaterials have been emerging as an alternative wastewater treatment technology (Ambashta and Sillanpaa, 2010). Magnetic nanomaterials can be easily separated using an external magnetic separation system after contaminants have been removed; hence, it is possible to preserve the inherent high selectivity of nanomaterials. Several studies have shown that magnetic nanoparticles (MNPs) could successfully support nanocomposites to remove organic and inorganic contaminants in wastewater (Lunge et al., 2014; Yu et al., 2013).

Layered double hydroxide (LDH) is an artificial anionic clay that is based on a structure of positively charged brucite-like layers, with interlayers of anions having water molecules (H_2O) (Wang and O'Hare, 2012). The general formula of LDH is $[M^{2+}_{1-x}M^{3+}_{x}(OH)_2]^{x+}(A^{n-})_{x/n} \cdot mH_2O$, where M^{2+} and M^{3+} are cationic metals, and A refers to anions such as carbonate (CO_3) or nitrate (NO_3). Previous studies have reported that LDH can effectively remove anionic contaminants such as As(V), phosphate, chromium, and Sb(V) via the ion exchange of interlayer anions (Goh et al., 2008). Furthermore, the thermal treatment of LDH has enhanced the removal efficiency of anionic contaminants due to its positively charged surface, which induces a charge imbalance by the elimination of interlayer substances (Goh et al., 2009). Furthermore, LDH has been applied as a substrate to support nanoparticles such as silver (Chen et al., 2012), graphene (Gao et al., 2011), TiO_2 (Lee et al., 2015), and Fe_3O_4 (Shao et al., 2012) in order to enhance the functionality of materials based on the large surface area of LDH.

In this study, magnetic functionalized LDH nanocomposite (MLDH) was prepared using well-known MNPs (γ-Fe_2O_3) in order to synthesize an effective separable material for use in an As(V) and Sb(V) removal system. Additionally, calcined MLDH (MLDO) was examined for the enhancement of As(V) and Sb(V) removal in water. The MLDO has potential for the in-situ field applications that require both the magnetic separation and removal of As(V) and Sb(V) in drinking water. Therefore, the physico-chemical properties of MLDO was examined, and the removal mechanisms of As(V) and Sb(V) by MLDO were investigated in this study.

2. Materials and methods

2.1. Preparation of MLDH and MLDO

Mg/Al LDH was first synthesized using a coprecipitation method in which 250 mL of Solution 1 (1 M Na_2CO_3 with 1 M NaOH) was dropwise added into 250 mL of Solution 2 (0.5 M $Mg(NO_3)_2$ 6 · H_2O and $Al(NO_3)_3$ $9H_2O$) until the pH of the mixture reached 9.5, and a white precipitate was obtained. The mixture was then aged for 48 h at 60 °C in a dry oven to increase its crystallinity. The precipitate was subsequently washed using deionized water, and then dried at 80 °C in a dry oven for 24 h before being stored in a desiccator prior to further use.

MNPs were also synthesized using a coprecipitation method (Yoon et al., 2015). In brief, a 250 mL mixed iron solution containing 0.1 M of ferrous chloride ($FeCl_2 \cdot 4H_2O$) and 0.2 M ferric chloride ($FeCl_3 \cdot 6H_2O$) (2:1 M ratio) was prepared. Then, 1 M NH_4OH was continuously added into the iron solution until the pH of the mixture reached 9.5, and a black precipitate was obtained. The black precipitate was washed using deionized water and dried at 80 °C in a dry oven for 24 h before being stored in a desiccator prior to further use. The process for preparing MLDO was described in our previous study (Lee et al., 2015) using flocculation method. Here, different ratio of Mg/Al LDH and well-dispersed MNPs were mixed into a 1 L bottle containing deionized water (The ratio of MNPs is 10 to 50%). The mixed solution was vigorously stirred by for 48 h at room temperature. The final slurry was then separated and calcined at 400 °C in a furnace which is the optimum calcination temperature for the removal of As(V) and Sb(V) by LDH and finally the samples were homogenized using a 100 mesh sieve.

2.2. Characterization

Powdered LDH, MNPs, MLDH and MLDO samples were prepared to investigate the physico-chemical properties. To investigate the crystallographic properties of MLDH and MLDO, powder XRD patterns were obtained using a high resolution X-ray diffractometer (HR-XRD, SIEMENS D5005 Diffractometer, Karlsruhe, Germany) combined with Cu

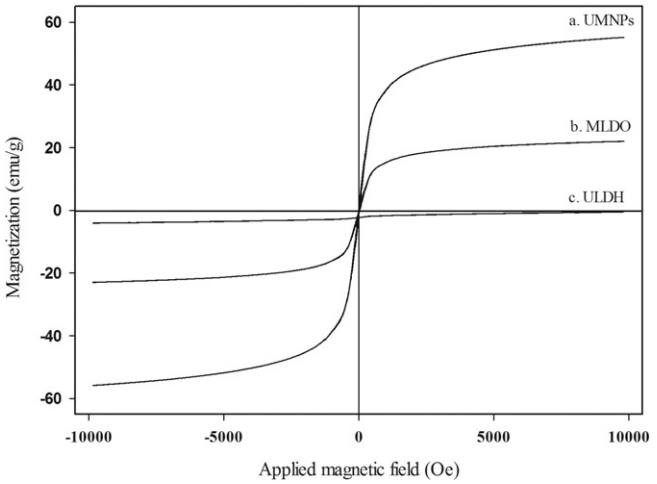

Fig. 2. Comparison of magnetic hysteresis loops of UMNPs (a), MLDO (b) and ULDH (c).

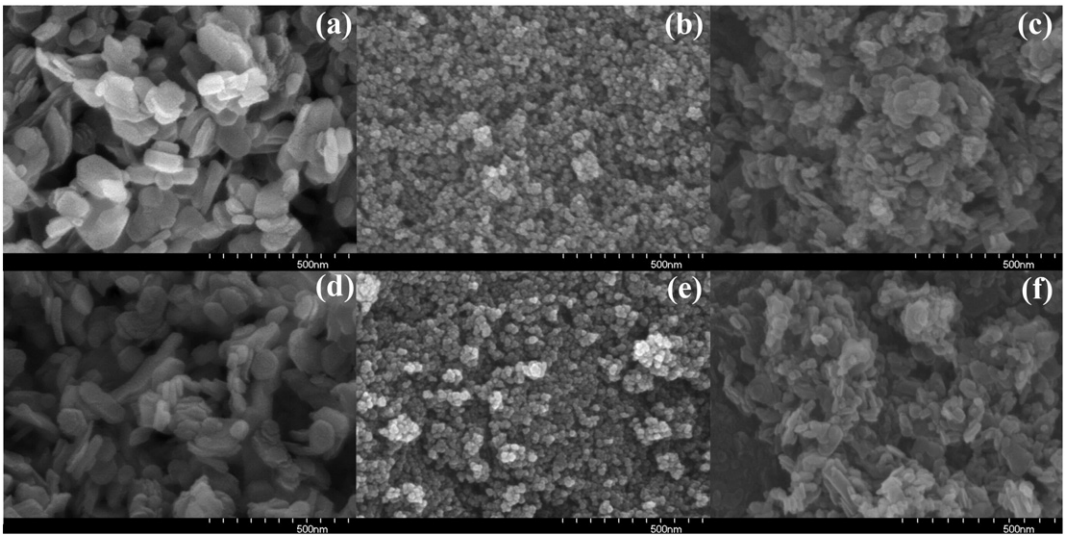

Fig. 3. Scanning electron microscope (SEM) images of ULDH (a), UMNPs (b), MLDH (c) and CLDH (d), CMNPs (e), MLDO (f).

Kα radiation (40 kV, 24 mA, 2θ: 5°–85°). The specific surface areas were measured using a BET analysis (ASAP2010, Micromeritics, USA), and the morphological characteristics and elemental composition of the samples were obtained using scanning electron microscope via elemental dispersive spectroscopy (FE-SEM; Hitachi S-4700, Japan). The saturated magnetism of MLDH and MLDO was then examined using a vibrating sample magnetometer (VSM; Lakeshore 665, USA). The chemical formation of MLDH and MLDO was analyzed using an X-ray photoelectron spectrometer (XPS; ESCA VG Multilab 2000, UK) and the information of functional groups in MLDO was obtained using FT-IR (Jasco-4600 plus, USA).

2.3. Removal of As(V) and Sb(V) using MLDO

All chemicals were reagent grade in the experiments. The 1000 mg/L stock solutions of As(V) and Sb(V) were prepared using $NaHAsO_4$ (Sigma Aldrich, USA) and $KSb(OH)_3$ (Sigma Aldrich, USA), respectively. Then, deionized water was used as needed to dilute the stock solutions. The initial concentrations of As(V) and Sb(V) in the batch experiments was adjusted to 50 mg/L, and the dose of MLDH and MLDO was 0.2 g/L. Powdered MLDH and MLDO was added into the As(V) and Sb(V) solutions and vigorously stirred at a constant temperature (25 °C) in a shaking incubator (HB-201SF, Hanbaek Science, Korea).

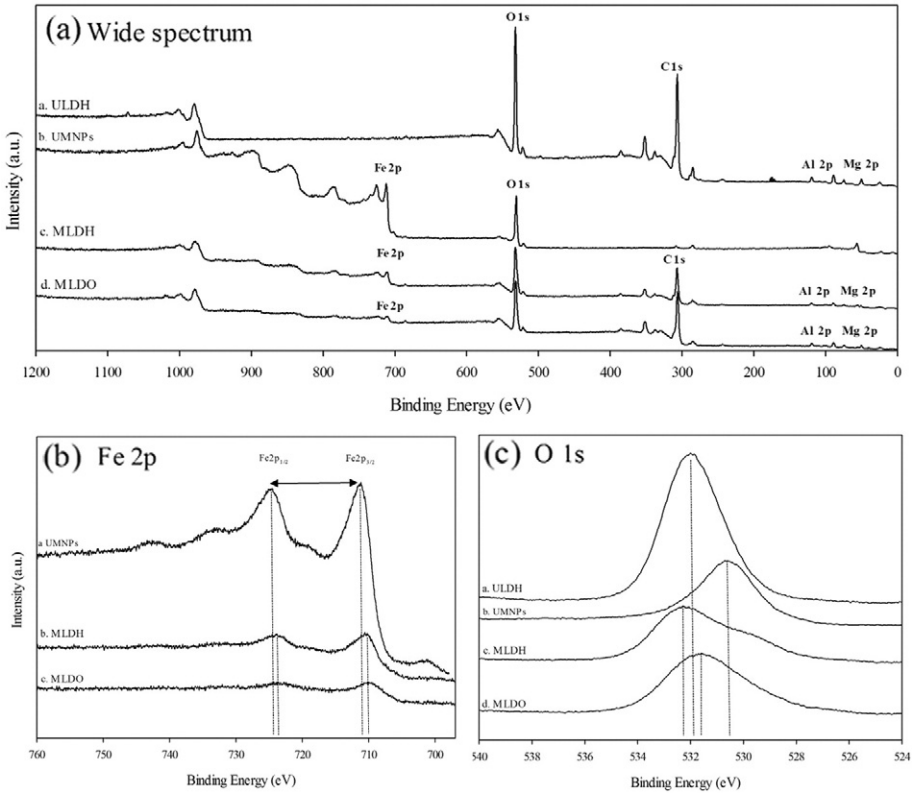

Fig. 4. X-ray photoelectron spectroscopy spectra of ULDH, UMNPs, MLDH and MLDO: wide spectrum (a), Fe 2p (b) and O 1s spectra (c).

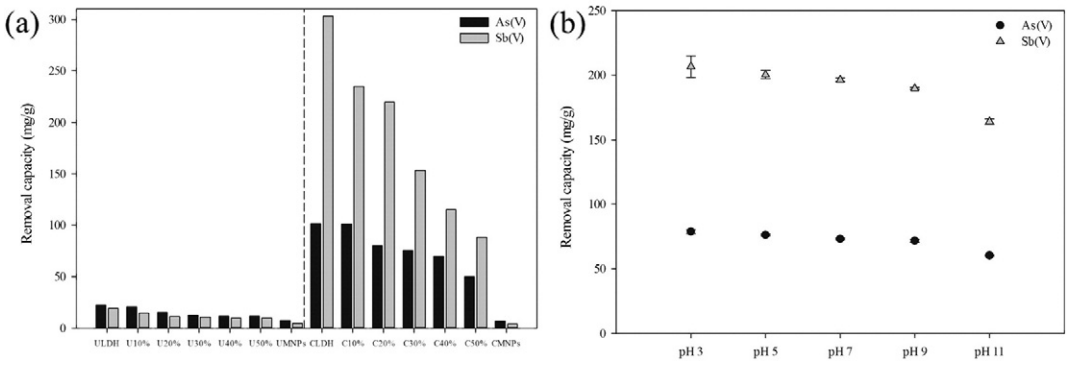

Fig. 5. Calcination effect for the removal of As(V) and Sb(V) (a) (ULDH, U: MLDH, CLDH, C: MLDO, UMNPs, CMNPs) and removal efficiency under different equilibrium pH (b) (sorbent: MLDO 20%).

The effect of pH was investigated under different pH conditions, which was adjusted from 3 to 11 using 0.1 M HCl (Sigma Aldrich, USA) and 0.1 M NaOH (Sigma Aldrich, USA). Kinetic tests were carried out as a function of reaction time (ranging from 5 min to 360 min). Isotherm experiments were conducted under As(V) and Sb(V) concentrations ranging from 10 mg/L to 500 mg/L. Finally, the data was fitted to the Langmuir and Freundlich isotherm model, and the maximum removal capacity was calculated.

The competitive effects of anionic co-ions were determined based on the presence of phosphate, sulfate, nitrite, nitrate, and carbonate. Each anion solution was prepared using NaH_2PO_4, Na_2SO_4, $NaNO_2$, $NaNO_3$, and $NaHCO_3$ (Sigma Aldrich, USA). The concentration of each anion was adjusted from 10 mg/L to 100 mg/L and 1000 mg/L of As(V) and Sb(V) solution. For the desorption experiments, used MLDO was mixed with 0.5 M NaOH and 5 M NaCl solutions and continuously stirred for 6 h. The MLDO was then washed using deionized water and a repetitive calcination process was conducted at 400 °C. Consecutive sorption, desorption, and regeneration studies were conducted in order to investigate the regenerability of MLDO.

3. Results and discussion

3.1. MLDH and MLDO characterization

Fig. 1(a) presents the X-ray diffraction patterns of uncalcined Mg/Al LDH (ULDH), calcined Mg/Al LDH(CLDH) at 400 °C, uncalcined MNPs (UMNPs), calcined MNPs at 400 °C (CMNPs), MLDH, and MLDO. The ULDH displays the typical structure of a layered double hydroxide, having basal reflections of (003), (006), (009), and (110) planes (Xia et al., 2013). In the CLDH, the typical Mg/Al peaks disappeared due to the collapse of the interlayer space, caused by the thermal treatment at 400 °C for 4 h. Fig. 1(c) shows the crystallographic structure of MNPs, the peaks located at (220), (311), (400), (511), and (440) planes were assigned to the mixture of γ-Fe_2O_3 and Fe_3O_4 (Yu et al., 2013). In this study, the both γ-Fe_2O_3 and Fe_3O_4 were designated as MNPs because both they were generally mixed, and the calcined MNPs did not display any phase change. As shown in Fig. 1(a) the MLDH and MLDO had entire peak patterns that were similar to both ULDH and γ-Fe_2O_3. The XRD patterns of the MLDO shows that the layered structure ((003), (006), (009), and (110) planes) decreased due to the elimination of water molecules in the interlayer space. Our previous study (Lee et al., 2015) confirmed that the calcination process decreased the interlayer space of LDH, the decreased interlayer space had the potential to remove anionic contaminants regardless of the presence of hybrid nanoparticles.

Fig. 1(b) displays the FT-IR spectra of the ULDH, CLDH, MNPs, MLDH and MLDO, in which absorption bands at 3450 cm^{-1} and 1350 cm^{-1} were observed in the ULDH. The band at 3450 cm^{-1} indicates the stretching vibrations in hydroxyl groups (−OH) in the brucite layers and interlayer water molecules (Das and Samal, 2004). The band at 1380 cm^{-1} can be assigned to the asymmetric stretching of interlayer carbonate anions (CO_3^-) (Lu et al., 2012). The CLDH represented that hydroxyl group almost disappeared after the thermal treatment, as incomplete peaks of carbonate remained. MLDH revealed that the hydroxyl and carbonate groups were restored due to the carbonate in water, whereas these peaks were eliminated in MLDO after the thermal treatment. MLDH revealed similar properties with ULDH, whereas there were no valid peaks in the uncalcined and calcined MNPs since their intensity was low.

Fig. 2 demonstrates the magnetic hysteresis loops of CLDH, MNPs, and MLDO. The data revealed that there is no magnetic effect by ULDH (<0.1 emu/g) and the maximum saturated magnetism of MNPs and MLDO were 63.2 emu/g and 21.6 emu/g, respectively. Although the

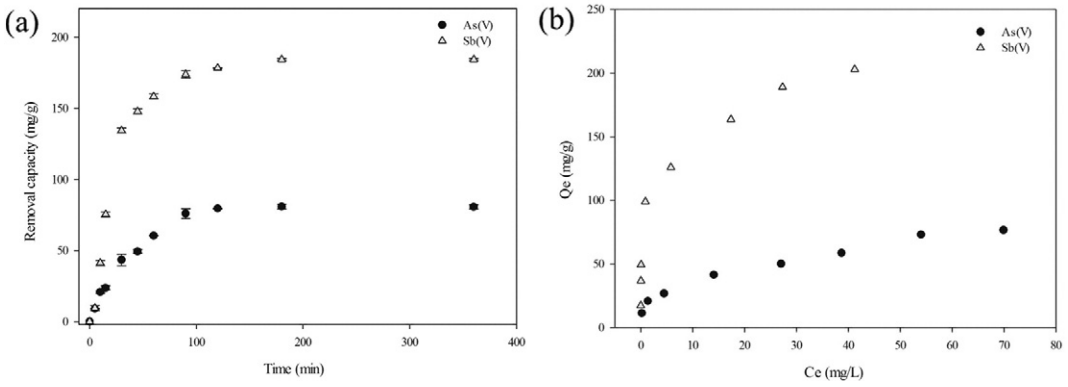

Fig. 6. Kinetic removal of As(V) and Sb(V) (a) and isotherm study by MLDO (b) (dose: 0.2 g/L, initial concentration of As(V) and Sb(V): 50 mg/L, initial pH: 7, reaction time: 24 h).

magnetism of MLDO decreased with the combination of non-magnetic Mg/Al LDH, it had effective magnetic properties compared with other magnetic materials, making it possible to apply in a separation system for water treatment facilities. Fig. 3 demonstrates the morphological characteristics of ULDH (Fig. 3(a)), MNPs (Fig. 3(b)), MLDH (Fig. 3(c)) and CLDH (Fig. 3(d)), MNPs (Fig. 3(e)), MLDO (Fig. 3(f)). The calcination process did not affect a change in the morphology. The ULDH and CLDH displayed a stacked plates-like form, and the average particle size of U was 100–150 nm. The MNPs had a globular form, and the average particle size was 30–50 nm. MLDH and MDLO had a combined form with Mg/Al LDH and MNPs and the average particle size was 150–200 nm.

Fig. 4 shows the XPS spectra of ULDH, MNPs, MLDH and MLDO; Fig. 4(a) presents the wide spectra of ULDH, MNPs, MLDH and MLDO. In Fig. 4(a), Mg 2p, Al 2p, C 1s, and O1s peaks were observed in ULDH at 50.4 eV, 74.8 eV, 285.2 eV, and 531.9 eV, respectively, and the wide spectra of MNPs have Fe $2p_{1/2}$ and $2p_{3/2}$ peaks at 724.7 eV and 711.2 eV. The wide spectra of MLDH and MLDO confirm the presence of MNPs on the surface of ULDH; the XPS results correspond to the XRD results. In the Fe 2p spectrum of MLDH and MLDO (Fig.4(b)), Fe $2p_{1/2}$ and $2p_{3/2}$ peaks were observed at 723.8 eV and 710. 3 eV, respectively. The shifting of Fe 2p peaks in MLDH and MLDO suggests there is a perceptible change in the chemical environment between ULDH and Fe (MNPs). Fig.4(c) presents O1s spectra of ULDH, MNPs, MLDH and MLDO at 531. 9 eV, 530.6 eV, 532.2 eV, and 531.6 eV, respectively. The shifting of O1s in MLDH and MLDO—in comparison with ULDH and MNPs—can be explained as being due to electron transfer because of the positively charged sheets of ULDH. Previous research (Zhu et al., 2015) reported that the binding energy of O1s in mixed oxide could be decreased by the ratio of magnetite. Consequently, the MNPs and ULDH undergo both physical and chemical interactions to form MLDH and MLDO.

3.2. As(V) and Sb(V) removal

The effect of calcination temperature on the removal of As(V) and Sb(V) by MLDH and MDLO was investigated based on several batch tests. The As(V) and Sb(V) removal experiments were conducted using ULDH, CLDH, MLDH, and MLDO (Fig. 5). Fig. 5(a) presents the batch experiment results of As(V) and Sb(V) removal, in which ULDH displays a removal capacity of 22.58 mg/g and 19.24 mg/g, respectively. To compare the As(V) removal capacity of different ratios of MNPs in MLDH and MLDO, batch removal experiments were conducted using different ratio of MNPs (10–50 wt.%) in MLDH and MLDO tested in removal experiments. In the MLDH, all samples displayed a lower removal capacity (<30 mg/g) than the MLDO in both As(V) and Sb(V). The figure shows that the removal capacities of As(V) and Sb(V) in MLDO dramatically increased, previous studies (Goh et al., 2009; Cheng et al., 2010) also reported that the calcination of LDH enhanced the removal capacity for anionic contaminants by the increase of potential sorption sites in the interlayer space of LDH. The removal capacity gradually decreased with an increase in the ratio of MNPs. This finding is due to the fact that the removal capacity for As(V) and Sb(V) by magnetic nanoparticles was enormously lower (<20 mg/g) than that of LDH (>100 mg/g). Fig. 5(b) illustrates the effect of pH on the removal of As(V) and Sb(V) by a load of 20% MNPs for MLDO. Both As(V) and Sb(V) show that the removal efficiency decreases with an increase in pH. In general, the removal efficiency of As(V) and Sb(V) under basic conditions is lower than under acidic and neutral conditions because the surface charge of MLDO has a lower positive charge under basic conditions (point of zero charge: 9.6).

Fig. 6(a) presents the results of kinetic removal of As(V) and Sb(V) by MLDO. The reaction rate was calculated using the pseudo-first and -second order kinetic models, with the results summarized in Table 2. Both kinetic models revealed a similar correlation coefficient (R^2: 0.963–0.992), and the data showed that the rate constants for Sb(V) removal are faster (K_1: 0.034, K_2: 1.87×10^{-4}) than for As(V) (K_1: 0.023, K_2: 2.80×10^{-4}). Therefore, MLDO was deemed to be more favorable for As(V) removal in terms of reaction rate, which can be also explained by its crystallographic affinity for Sb(V) (Table 1).

Table. 1
Pseudo 1st and 2nd order kinetic parameters for As(V) and Sb(V) removal by MLDO.

	Pseudo 1st order			Pseudo 2nd order		
Contaminants	q_e (mg/g)	k_1 (min^{-1})	R^2	q_e (mg/g)	k_2 (g mg^{-1} min^{-1})	R^2
As(V)	82.31	0.023	0.992	96.67	2.80×10^{-4}	0.978
Sb(V)	184.02	0.034	0.983	213.2	1.87×10^{-4}	0.963

The isotherm experiment data was fitted by Langmuir and Freundlich isotherm model. The constants for the Langmuir and Freundlich models are summarized in Table 2 and Fig. 6(b), which illustrate the adsorption isotherm model for As(V) and Sb(V) by MLDO. From the Langmuir isotherm, the calculated maximum adsorption capacities for As(V) and Sb(V) were 83.01 mg/g and 180.96 mg/g, respectively. Both sets of data show that the Freundlich model has a better fit than the Langmuir isotherm model, indicating that the multilayer sorption mechanism in MLDO can be more favorable than that of monolayer sorption processes.

3.3. Removal mechanism of As(V) and Sb(V) using MLDO

To investigate the removal mechanisms of As(V) and Sb(V) for MLDO, the surface state of MLDO was examined using XPS, XRD, and FT-IR after reaction with As(V) and Sb(V). In the XPS spectrum, Al2p of MLDO with As(V) and Sb(V) was compared (Fig. 7(a)), additionally As 3d and Sb 3d peaks were observed on the MLDO, thus confirmed that the sorption of As(V) and Sb(V) by MLDO. In As 3d (Fig. 7(b)) and O1s with Sb 3d spectra (Fig. 7(c)), a clear sorption of As(V) and Sb(V) are observed (Lu et al., 2015; Vithanage et al., 2015), as well as a significant alteration of the constituents of O1s in both the As(V) and Sb(V) samples. The binding energy of Al 2p spectra in MLDO slightly changed by the reaction with As(V) and Sb(V) (74.0 eV to 74.4 eV). Previously, Goh et al. (2009) reported that Al and O atoms are involved in the sorption of As(V) and Sb(V), and that the active groups of the Al surface play an important role for the sorption of As(V) and Sb(V) in LDH; possible inner-sphere complexes can be assumed to form at the Al^{3+} center in MLDO. The XRD results (Fig. 7(d)) show the position of sorbed As(V) and Sb(V) in MLDO, with the increase of the d_{003} peak indicating that the As(V) and Sb(V) combined in the interlayer space. Interestingly, a brandholzite-like peak was observed in the Sb(V) samples, indicating that there is an additional complex between the magnesium and Sb(V) (Kameda et al., 2011). The FT-IR data further revealed that the hydroxyl peaks (3450 cm^{-1}) were restored in both the As(V) and Sb(V) sorbed samples (Fig. 7(e)). Although the specific As—O and Sb—O peaks cannot be distinguished in the data, it might be expected that most forms of As(V) and Sb(V) are present as M-OH forms in MLDO. Consequently, As(V) and Sb(V) may be present in hydroxyl form in the interlayer space.

Table. 2
Langmuir and Freundlich adsorption isotherm for As(V) and Sb(V) by MLDO.

			Contaminants	
Isotherm	Equation	Parameters	As(V)	Sb(V)
Langmuir	$q = q_m bC/(1 + bC)$	qm, L (mg/g)	83.01	180.96
		K_L (L/mg)	0.084	1.358
		R^2	0.900	0.866
Freundlich	$(q = K_F C^{1/n})$	K_F (g/mg·L)	15.99	90.19
		1/n	0.366	0.218
		R^2	0.987	0.991

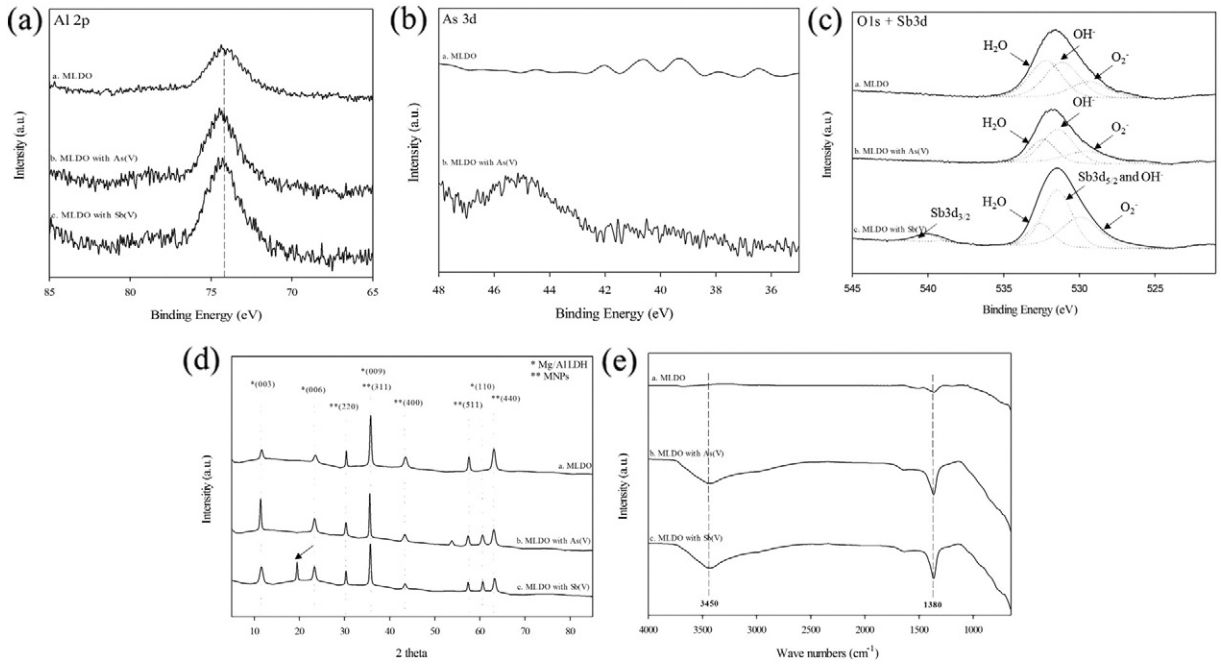

Fig. 7. XPS spectra of MLDO for Al 2p (a), As 3d (b), O1s with Sb 3d (c), X-ray diffraction for rehydration effect of MLDO with As(V) and Sb(V) (d), change of Fourier-transform infrared spectra by rehydration of MLDO with As(V) and Sb(V) (e).

3.4. Competitive anion effect and regenerability of MLDO

Competitive anion effects on the removal of As(V) and Sb(V) by chloride, sulfate, nitrate, carbonate and phosphate by MLDO are shown in Fig. 8, where it is clear that Cl^- and NO_3^- did not markedly inhibit the As(V) and Sb(V) removal. In general, divalent anions are more competitive with As(V) and Sb(V) than monovalent anion species. When adding CO_3^{2-} and SO_4^{3-} from 100 mg/L, the removals of As(V) and Sb(V) were inhibited by around 15% and 10%, respectively. We posit that the effect of CO_3^{2-} and SO_4^{3-} could be caused by the formation of complexes with As(V) and Sb(V) on the MLDO surface (Lu et al., 2015). In both As(V) and Sb(V), phosphate significantly affected the removal of As(V) and Sb(V) from 100 mg/L. In addition, the ionic radii of PO_4 (0.17 Å) is significantly smaller than that of As(V) (0.36 Å) and Sb(V) (0.62 Å) because the length of its P—O bond is shorter. Therefore, phosphate ions have a stronger charge density than As(V) and Sb(V) ions (Awual et al., 2011). The driving force for the removal of As(V) and Sb(V) by MLDO can originate from the electrostatic attraction between anions and positively charged MLDO (point of zero charge: 9.6). Consequently, the presence of PO_4 ions can interfere with the sorption of As(V) and Sb(V) by MLDO (Fig. 9).

To consider its practical applicability, repetitive regenerability tests of MLDO were conducted using 0.5 M NaOH and 5 M NaCl. In the first sorption, the removal capacity of As(V) and Sb(V) by MLDO was 82 mg/g and 181 mg/g, respectively. In the first regeneration cycle, it was observed that the removal efficiency clearly decreased for both As(V) and Sb(V). However, the regeneration efficiency of As(V) was maintained at about 70% for five cycles, whereas the regeneration of Sb(V) and its regeneration efficiency significantly decreased in the fifth cycle. In terms of As(V), the ion exchange process between As(V) and NaOH with Cl^- ions significantly affected the regeneration efficiency. Notably, the Sb(V) regeneration rate can be negatively influenced by the formation of a brandholzite-like structure between MLDO and Sb(V); i.e., crystallization influences the sorption and desorption of Sb(V) on LDH in MLDO, whereas MNPs do not significantly affect the sorption and desorption because the ratio is low in MLDO. The comparisons of the removal capacities among MDLO and other reported magnetic materials are summarized in Table 3. Among these materials, our

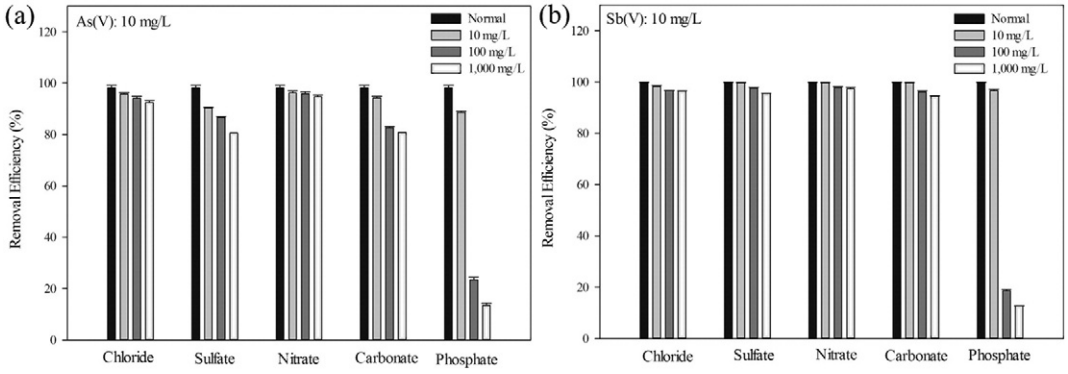

Fig. 8. Competitive co-exist anion effect on the removal of As(V) (a) and Sb(V) (b) by MLDO (initial concentration of As(V) and Sb(V): 10 mg/L, anion concentration: 10, 100 and 1000 mg/L).

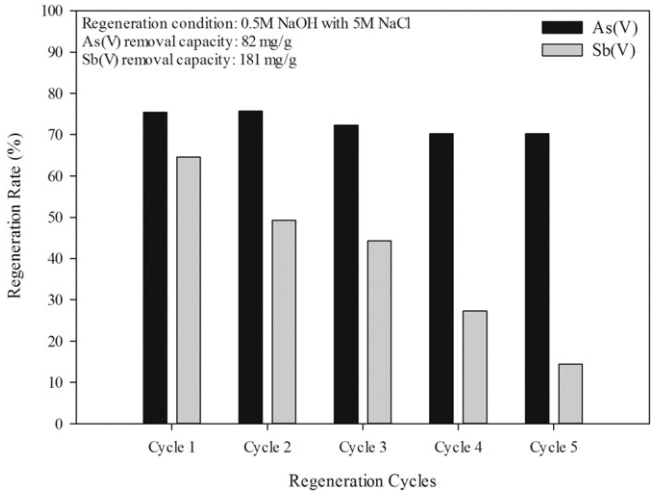

Fig. 9. Regenerability of MLDO for As(V) and Sb(V) (desorption condition: 0.5 M NaOH with 5 M NaCl, sorption condition: pH 7, dose: 0.2 g/L, initial concentration of As(V) and Sb(V): 50 mg/L).

studies also confirmed the effective removal of As(V) and Sb(V) by MLDO. In addition the optimized regeneration conditions in our study increased the practical applicability of MLDO, with its high removal capacity compared to other materials.

4. Conclusion

To synthesize a novel magnetic nanocomposite, MNPs supported calcined layered double oxide (MLDO) was successfully prepared. The synthesized MLDO demonstrated a saturated magnetism of 21.6 emu/g, and good separation properties. SEM data revealed that the MNPs (<50 nm) were attached onto the LDH surface (around 100 nm). The supported MNPs stably attached on the surface of LDH, and XPS data further revealed that MNPs were chemically combined with the LDH. The MLDO enhanced the removal capacity by increasing the interlayer space used to implement the reconstruction process for As(V) and Sb(V). Neutral and acidic pH conditions were found to be more favorable for the removal of As(V) and Sb(V) than alkaline conditions. In addition, Sb(V) was more rapidly removed by MLDO than As(V), and the maximum removal capacities of As(V) and Sb(V) by 20% MLDO were 83.01 mg/g and 180.96 mg/g, respectively. Al atoms in MLDO played an important role in the removal mechanism by forming an inner-sphere complex, and the As(V) and Sb(V) combined as a hydroxyl form in the interlayer space in MLDO. The regeneration of As(V) was maintained at around 70% for five cycles using 0.5 M NaOH and 5 M NaCl solutions. Although the Sb(V) regeneration was limited for two cycles (~50%), the high Sb(V) removal capacity overcame the disadvantage of regenerability. Consequently, MLDO could be an economical option for the removal system of As(V) and Sb(V) in water treatments considering competitive effect, maximum sorption capacity and regeneration rate, based on both magnetic separability.

Table 3
Comparison of removal capacity among MDLH and other reported magnetic materials.

Target	Material	Removal capacity (mg/g)	pH	Ref.
As(V)	Sawdust/$MnFe_2O_4$ composite	88.9	7.0	Podder and Majumder (2016)
	ZVI-resin composite	125	6.5	Du et al. (2013)
	Zn/Fe LDH	151.0	7.0	Lu et al. (2015)
	Fe-Cu binary oxide	82.7	7.0	Chang et al. (2013)
	MLDO	83.0	7.0	This study
Sb(V)	Potassium ferrate	129.0	6.5	Lan et al. (2016)
	Zero valent iron	39.8	7.1	Li et al. (2015)
	Fe-Mn binary oxide	169.4	5.0	Lu et al. (2015)
	Zn/Fe LDH	122.0	7.0	Lu et al. (2015)
	MLDO	180.9	7.0	This study

Acknowledgements

This research was financially supported by Brain Korea 21 of School of Environmental Science and Engineering at Gwangju Institute of Science and Technology (GIST), Korea.

References

Ambashta, R.D., Sillanpaa, M., 2010. Water purification using magnetic assistance: A review. J. Hazard. Mater. 180:38–49. http://dx.doi.org/10.1016/j.jhazmat.2010.04.105.
Awual, M.R., El-Safty, S.A., Jyo, A., 2011. Removal of trace arsenic(V) and phosphate from water by a highly selective ligand exchange adsorbent. J. Environ. Sci. 23, 1947–1954.
Chang, G., Ren, Z., Zhang, X., Chen, J., 2013. Nanostructured iron(III)-copper(II) binary oxide: A novel adsorbent for enhanced arsenic removal from aqueous solutions. Water Res. 47, 4022–4031.
Chanpiwat, P., Sthiannopkao, S., Cho, K.H., Kim, K.-W., San, V., Suvanthong, B., Vongthavady, C., 2011. Contamination by arsenic and other trace elements of tube-well water along the Mekong River in Lao PDR. Environ. Pollut. 159, 567–576.
Chen, C., Gunawan, P., Lou, X.W., Xu, R., 2012. Silver nanoparticles deposited layered double hydroxide nanoporous coatings with excellent antimicrobial activities. Adv. Funct. Mater. 22:780–787. http://dx.doi.org/10.1002/adfm.201102333.
Cheng, X., Huang, X., Wang, X., Sun, D., 2010. Influence of calcination on the adsorptive removal of phosphate by Zn-Al layered double hydroxides from excess sludge liquor. J. Hazard. Mater. 177:516–523. http://dx.doi.org/10.1016/j.jhazmat.2009.12.063.
Chowdhury, U.K., Biswas, B.K., Chowdhury, T.R., Samanta, G., Mandal, B.K., Basu, G.C., Chanda, C.R., Lodh, D., Saha, K.C., Mukherjee, S.K., Roy, S., Kabir, S., Quamruzzaman, Q., Chakraborti, D., 2000. Groundwater arsenic contamination in Bangladesh and West Bengal, India. Environ. Health Perspect. 108:393–397. http://dx.doi.org/10.2307/3454378.
Das, N., Samal, A., 2004. Synthesis, characterisation and rehydration behaviour of titanium(IV) containing hydrotalcite like compounds. Microporous Mesoporous Mater. http://dx.doi.org/10.1016/j.micromeso.2004.04.004.
Du, Q., Zhang, S., Pan, B., Lv, L., Zhang, W., Zhang, Q., 2013. Bifunctional resin-ZVI composites for effective removal of arsenite through simultaneous adsorption and oxidation. Water Res. 47:6064–6074. http://dx.doi.org/10.1016/j.watres.2013.07.020.
Filella, M., Belzile, N., Chen, Y., 2002. Antimony in the environment: a review focused on natural waters I. Earth-Sci. Rev. 57:125–176. http://dx.doi.org/10.1016/S0012-8252(01)00070-8.
Gao, Z., Wang, J., Li, Z., Yang, W., Wang, B., Hou, M., He, Y., Liu, Q., Mann, T., Yang, P., Zhang, M., Liu, L., 2011. Graphene nanosheet/Ni^{2+}/Al^{3+} layered double-hydroxide composite as a novel electrode for a supercapacitor. Chem. Mater. 23:3509–3516. http://dx.doi.org/10.1021/cm200975x.
Goh, K.-H., Lim, T.-T., Dong, Z., 2009. Enhanced arsenic removal by hydrothermally treated nanocrystalline Mg/Al layered double hydroxide with nitrate intercalation. Environ. Sci. Technol. 43:2537–2543. http://dx.doi.org/10.1021/es802811n.
Goh, K.-H., Lim, T.-T., Dong, Z., 2008. Application of layered double hydroxides for removal of oxyanions: a review. Water Res. 42, 1343–1368.
Hanh, H.T., Kim, K.-W., Bang, S., Hoa, N.M., 2011. Community exposure to arsenic in the Mekong river delta, Southern Vietnam. J. Environ. Monit. 13:2025–2032. http://dx.doi.org/10.1039/c1em10037h.
He, M., 2007. Distribution and phytoavailability of antimony at an antimony mining and smelting area, Hunan, China. Environ. Geochem. Health 29:209–219. http://dx.doi.org/10.1007/s10653-006-9066-9.
Jana, U., Chassany, V., Bertrand, G., Castrec-Rouelle, M., Aubry, E., Boudsocq, S., Laffray, D., Repellin, A., 2012. Analysis of arsenic and antimony distribution within plants growing at an old mine site in Ouche (Cantal, France) and identification of species suitable for site revegetation. J. Environ. Manag. 110:188–193. http://dx.doi.org/10.1016/j.jenvman.2012.06.007.
Kameda, T., Honda, M., Yoshioka, T., 2011. Removal of antimonate ions and simultaneous formation of a brandholzite-like compound from magnesium–aluminum oxide. Sep. Purif. Technol. 80:235–239. http://dx.doi.org/10.1016/j.seppur.2011.04.032.
Lan, B., Wang, Y., Wang, X., Zhou, X., Kang, Y., Li, L., 2016. Aqueous arsenic (As) and antimony (Sb) removal by potassium ferrate. Chem. Eng. J. 292, 389–397.
Lee, S.-H., Kim, K.-W., Choi, H., Takahashi, Y., 2015. Simultaneous photooxidation and sorptive removal of As(III) by TiO_2 supported layered double hydroxide. J. Environ. Manag. 161:228–236. http://dx.doi.org/10.1016/j.jenvman.2015.06.049.
Li, J., Bao, H., Xiong, X., Sun, Y., Guan, X., 2015. Effective Sb(V) immobilization from water by zero-valent iron with weak magnetic field. Sep. Purif. Technol. 151, 276–283.
Lu, H., Zhu, Z., Zhang, H., Zhu, J., Qiu, Y., 2015. Simultaneous removal of arsenate and antimonate in simulated and practical water samples by adsorption onto Zn/Fe layered double hydroxide. Chem. Eng. J. 276:365–375. http://dx.doi.org/10.1016/j.cej.2015.04.095.
Lu, R., Xu, X., Chang, J., Zhu, Y., Xu, S., Zhang, F., 2012. Improvement of photocatalytic activity of TiO_2 nanoparticles on selectively reconstructed layered double hydroxide. Appl. Catal. B Environ. 111–112:389–396. http://dx.doi.org/10.1016/j.apcatb.2011.10.022.

Lunge, S., Singh, S., Sinha, A., 2014. Magnetic iron oxide (Fe_3O_4) nanoparticles from tea waste for arsenic removal. J. Magn. Magn. Mater. 356:21–31. http://dx.doi.org/10.1016/j.jmmm.2013.12.008.

McCarty, K.M., Hanh, H.T., Kim, K.-W., 2011. Arsenic geochemistry and human health in South East Asia. Rev. Environ. Health 26, 71–78.

Mohan, D., Pittman, C.U., 2007. Arsenic removal from water/wastewater using adsorbents—a critical review. J. Hazard. Mater. 142, 1–53.

Phan, K., Phan, S., Huoy, L., Suy, B., Wong, M.H., Hashim, J.H., Mohamed Yasin, M.S., Aljunid, S.M., Sthiannopkao, S., Kim, K.W., 2013. Assessing mixed trace elements in groundwater and their health risk of residents living in the Mekong River basin of Cambodia. Environ. Pollut. 182:111–119. http://dx.doi.org/10.1016/j.envpol.2013.07.002.

Podder, M.S., Majumder, C.B., 2016. Fixed-bed column study for As(III) and As(V) removal and recovery by bacterial cells immobilized on Sawdust/$MnFe_2O_4$ composite. Biochem. Eng. J. 105, 114–235.

Ray, P.Z., Shipley, H.J., 2015. Inorganic nano-adsorbents for the removal of heavy metals and arsenic: a review. RSC Adv. 5:29885–29907. http://dx.doi.org/10.1039/C5RA02714D.

Shao, M., Ning, F., Zhao, J., Wei, M., Evans, D.G., Duan, X., 2012. Preparation of Fe_3O_4@SiO_2@Layered Double Hydroxide Core-Shell Microspheres for Magnetic Separation of Proteins (Jacs).

Smedley, P., Kinniburgh, D., 2002. A review of the source, behaviour and distribution of arsenic in natural waters. Appl. Geochem. 17, 517–568.

Smith, A.H., Lingas, E.O., Rahman, M., 2000. Contamination of drinking-water by arsenic in Bangladesh: a public health emergency. Bull. World Health Organ. 78:1093–1103. http://dx.doi.org/10.1590/S0042-96862000000900005.

Sundar, S., Chakravarty, J., 2010. Antimony toxicity. Int. J. Environ. Res. Public Health 7:4267–4277. http://dx.doi.org/10.3390/ijerph7124267.

USEPA, 2001. National primary drinking water regulation: arsenic and clarifications to compliance and new source contaminants monitoring: final rule. Fed. Regist. 66, 6976–7066.

Vithanage, M., Rajapaksha, A.U., Ahmad, M., Uchimiya, M., Dou, X., Alessi, D.S., Ok, Y.S., 2015. Mechanisms of antimony adsorption onto soybean stover-derived biochar in aqueous solutions. J. Environ. Manag. 151:443–449. http://dx.doi.org/10.1016/j.jenvman.2014.11.005.

Wang, Q., O'Hare, D., 2012. Recent advances in the synthesis and application of layered double hydroxide (LDH) nanosheets. Chem. Rev. 112:4124–4155. http://dx.doi.org/10.1021/cr200434v.

WHO, 2003. Antimony in Drinking-water. Background Document for Development of WHO Guidelines for Drinking-Water Quality. WHO (doi:WHO/SDE/WSH/03.04/74).

Xia, S.-J., Liu, F.-X., Ni, Z.-M., Xue, J.-L., Qian, P.-P., 2013. Layered double hydroxides as efficient photocatalysts for visible-light degradation of rhodamine B. J. Colloid Interface Sci. 405:195–200. http://dx.doi.org/10.1016/j.jcis.2013.05.064.

Xu, T., Kamat, P., O'Shea, K., 2005. Mechanistic evaluation of arsenite oxidation in TiO_2 assisted photocatalysis. J. Phys. Chem. A 9070–9075.

Yoon, Y., Park, W.K., Hwang, T.-M., Yoon, D.H., Yang, W.S., Kang, J.-W., 2015. Comparative evaluation of magnetite-graphene oxide and magnetite-reduced graphene oxide composite for As(III) and As(V) removal. J. Hazard. Mater. http://dx.doi.org/10.1016/j.jhazmat.2015.10.053.

Yu, L., Peng, X., Ni, F., Li, J., Wang, D., Luan, Z., 2013. Arsenite removal from aqueous solutions by γ-Fe_2O_3-TiO_2 magnetic nanoparticles through simultaneous photocatalytic oxidation and adsorption. J. Hazard. Mater. 246–247:10–17. http://dx.doi.org/10.1016/j.jhazmat.2012.12.007.

Zhu, S., Fang, S., Huo, M., Yu, Y., Chen, Y., Yang, X., Geng, Z., Wang, Y., Bian, D., Huo, H., 2015. A novel conversion of the groundwater treatment sludge to magnetic particles for the adsorption of methylene blue. J. Hazard. Mater. 292:173–179. http://dx.doi.org/10.1016/j.jhazmat.2015.03.028.